Available online at www.sciencedirect.com
SCIENCE DIRECT®
Journal of Power Sources 142 (2005) 30–42
JOURNAL OF POWER SOURCES
www.elsevier.com/locate/jpowsour

Performance analysis of a tubular solid oxide fuel cell/micro gas turbine hybrid power system based on a quasi-two dimensional model

Tae Won Song[a], Jeong Lak Sohn[a,*], Jae Hwan Kim[b], Tong Seop Kim[c], Sung Tack Ro[a], Kenjiro Suzuki[d]

[a] *School of Mechanical and Aerospace Engineering, Seoul National University, San 56-1 Shilim-Dong, Gwanak-Gu, Seoul 151-742, Republic of Korea*
[b] *Turbomachinery Branch, Korea Aerospace Research Institute, 45 Eoeun-Dong, Yusung-Gu, Daejeon 305-333, Republic of Korea*
[c] *School of Mechanical Engineering, Inha University, 253 Yonghyun-Dong, Nam-Gu, Incheon 402-752, Republic of Korea*
[d] *Department of Machinery and Control Systems, Shibaura Institute of Technology, 307 Fukasaku, Saitama 337-8570, Japan*

Received 3 August 2004; accepted 9 October 2004
Available online 8 December 2004

Abstract

A quasi-two dimensional (quasi-2D) model is proposed as a tool to predict the performance of solid oxide fuel cell (SOFC) system composed of bundles of tubular SOFCs and internal reformers. The model is developed by considering heat and mass transfer characteristics mainly along the longitudinal direction of the system, and the electrochemical reaction in its perpendicular direction. With this model, the temperature distribution in the fuel and the air streams along the longitudinal direction of the bundles of tubular SOFCs and internal reformers can be easily predicted. The predicted cell temperature along the longitudinal direction of the tubular SOFC shows important phenomena, which include the temperature rise near the entrance of the fuel cell by the electrochemical reaction and its decrease due to heat transferred from the fuel cell to the internal reformer that absorbs heat in reforming reactions. Also, it is found that different system arrangements and component characteristics influence significantly the heat-transfer characteristics, and possibly the system performance. The results from the quasi-2D model are applied to the performance analysis of a tubular SOFC/micro gas turbine (MGT) hybrid system.

Keywords: Solid oxide fuel cell; Micro gas turbine; Hybrid system; Performance analysis; Heat and mass transfer; Model

1. Introduction

Fuel cells are considered to be good candidates for next-generation power sources because of their high-thermal efficiencies and ultra-low emissions. The performance characteristics of a fuel cell are greatly dependent on its operating temperature. Low-temperature types such as the proton exchange membrane fuel cell (PEMFC) are suitable for automotive applications because of their relatively rapid response to varying load demands. On the other hand, high-temperature types such as the molten carbonate fuel cell (MCFC) and the solid oxide fuel cell (SOFC) are suitable for stationary power-generation systems due to their high-thermal efficiency. Another important advantage of a high-temperature fuel cell comes from the high-temperature exhaust gas, which can be used as an additional heat source for other purposes [1]. In a solid oxide fuel cell/micro gas turbine (MGT) hybrid power system, the high-temperature exhaust gas of the SOFC is used as the source of energy for operating the micro gas turbine to boost power with the same fuel consumption. The theoretical feasibilities of such hybrid power systems have been investigated by numerous research groups since the mid-1990s. Harvey and Richter [2], who proposed a hybrid thermodynamic cycle combining a gas turbine and a fuel cell, are the

* Corresponding author. Tel.: +82 2 880 7434; fax: +82 2 889 6205.
E-mail addresses: singlee@plaza1.snu.ac.kr (T.W. Song), jlsohn@snu.ac.kr (J.L. Sohn), kjaehwan@kari.re.kr (J.H. Kim), kts@inha.ac.kr (T.S. Kim), stro@snu.ac.kr (S.T. Ro), ksuzuki@sic.shibaura-it.ac.jp (K. Suzuki).

0378-7753/$ – see front matter © 2004 Elsevier B.V. All rights reserved.
doi:10.1016/j.jpowsour.2004.10.011

Nomenclature

A	active area (m^2)
d	thickness (m)
D	diameter (m)
E_N	Nernst potential (V)
F	Faraday constant
g	molar Gibbs free energy (kJ kmol^{-1})
$\underline{h}$	heat transfer coefficient (kW m^{-2} K^{-1})
$\overline{h}$	molar enthalpy (kJ kmol^{-1})
LHV	lower heating value of CH_4 (kJ kmol^{-1})
$\dot{n}$	molar flow rate (kmol s^{-1})
N	number of segments
p	pressure (kPa)
Q	heat transfer rate (kW)
RR	recirculation rate
SCR	steam–carbon ratio
T	temperature (K or °C)
U	utilization factor
V_{act}	activation polarization (V)
V_c	operating cell voltage (V)
V_{ohm}	ohmic loss (V)
w	width (m)
W_{fc}	electrical work (kW)

Greek

ε	emissivity
ρ	resistivity (Ω m)
σ	Stefan–Boltzmann constant (W m^{-2} K^{-4})

Subscript

a	air gas or anode
c	fuel cell or cathode
e	electrolyte
f	fuel gas
int	interconnection
r	reforming fuel gas
rw	reformer wall
fp	fuel feed passage
ft	air feed tube

pioneers in this area. In the technical evolution of the fuel cell/gas turbine hybrid power system, both SOFCs [3] and MCFCs [4] have been considered as possible candidates for the fuel cell. Recent studies have, however, focused on the SOFC because of its higher thermal efficiency [5].

In 2001, Siemens–Westinghouse successfully demonstrated a 100-kW class tubular SOFC-based cogeneration power system. That work was followed by the development of a 220-kW class tubular SOFC/MGT hybrid power system [6]. A demonstration unit developed by Siemens–Westinghouse has been undergoing performance trials at the National Fuel Cell Research Center (NFCRC) of the University of California, USA, since 2000 [6,7]. Other reports of the Siemens–Westinghouse systems have also been published [8–10].

In spite of the introduction of many innovative cycles for the SOFC/MGT hybrid power system, its universal configuration is not yet fully established. Studies to develop new system configurations for better performance are still in progress. Performance analysis of the hybrid system using mathematical models is an essential tool to investigate the performance and operational characteristics of the various configurations. Mathematical thermodynamic models of the SOFC/MGT hybrid power system have been developed by numerous research groups. Among them, Massardo and Lubelli [5] investigated the characteristics of the design point performance of an internal reforming SOFC/MGT hybrid power system. Kim and Suzuki [11] conducted a similar study but used different mathematical models. Their models were recently improved by taking into consideration other physical phenomena of practical importance such the heat transfer inside the SOFC [12].

In the present study, a new model is proposed to enhance the accuracy of the performance analysis of a tubular SOFC/MGT hybrid power system by taking into account the length effect of tubular SOFCs. In addition, the model can be applied for different configurations and/or characteristics of the system components.

2. System configurations

A schematic diagram of the tubular SOFC/MGT hybrid power system under investigation is given in Fig. 1(a). It is the same as that of the Siemens–Westinghouse design [6,7]. The SOFC module is divided into two parts, namely, bundles of tubular SOFCs and reformers. A bundle of tubular SOFCs is composed of tubes with a length of 150 cm and a diameter of 2.2 cm [13,14]. Each tubular SOFC is sealed only at one end. The wall of the tubular SOFC comprises three layers: cathode (inner wall), electrolyte, and anode (outer wall). On the other hand, the MGT module is composed of a compressor, a combustor, a turbine, and a recuperator that represents a regenerative Brayton cycle.

The compressed fuel (methane) is fed into the reformers, i.e., a pre-reformer and an indirect internal reformer, and is then supplied to the anode side of each tubular SOFC. Ambient air is compressed by a compressor that is driven by the turbine, and then heated in the recuperator by the hot gas stream from the turbine exhaust. High-temperature and high-pressure air enters the cathode side of each tubular SOFC, and electrochemically reacts with fuel supplied from the anode side in the wall of each tubular SOFC. Exhaust gas from the SOFC module is burnt in the combustor to raise its temperature and expanded by the turbine in the MGT module to produce shaft power. Since the SOFC module is operated under high-pressure conditions, the system is called a ‘pressurized hybrid system’.

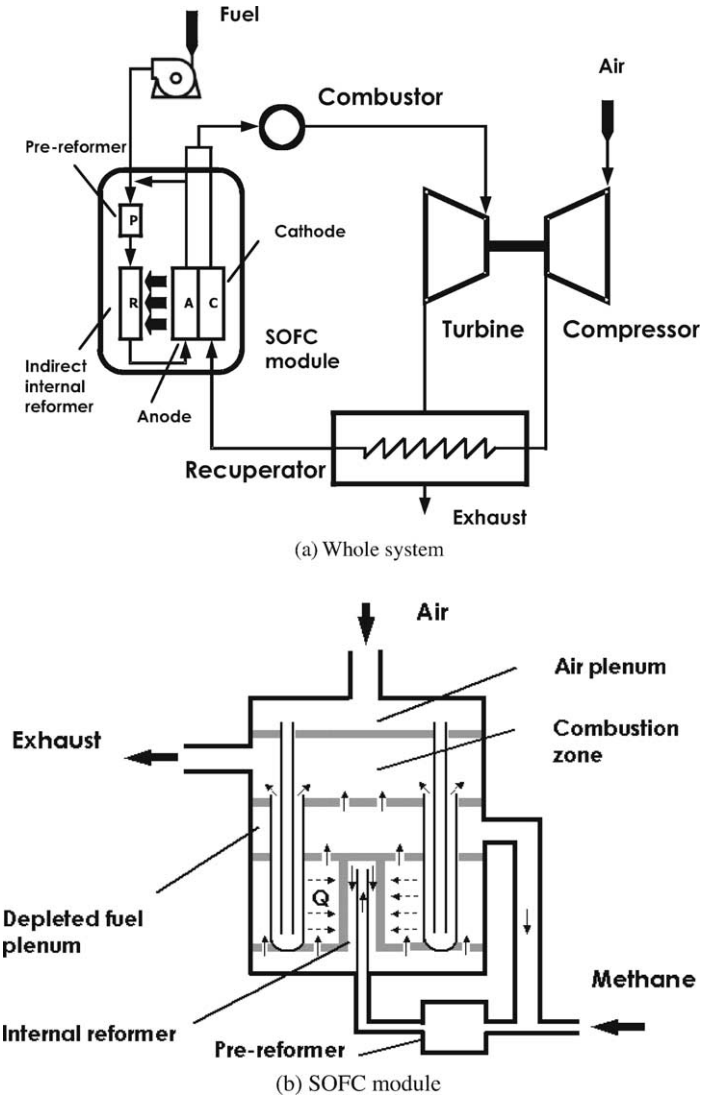

Fig. 1. Schematic diagrams of tubular SOFC/MGT hybrid power system: (a) whole system and (b) SOFC module.

The fuel and air streams in the SOFC module are shown in Fig. 1(b) and include a pre-reformer, an indirect internal reformer, the SOFC bundles, and a combustor. Here, the combustor can be treated either as an afterburner in the SOFC module or a combustor in the MGT. After being reformed in both the pre-reformer and the indirect internal reformer, the fuel that enters the SOFC module flows along the outside of each tubular SOFC from the sealed bottom towards the open end. This fuel is then partially reformed in the pre-reformer so as to reduce the reforming load of the internal reforming process. Here, the latter process is defined as the reforming process, which uses the generated heat from the fuel cell. There are two types of reforming process: (i) a process in an indirect internal reformer, which is located outside of the fuel cell and (ii) a direct internal reforming process in the anode of the fuel cell. Partially reformed fuel at the exit of the pre-reformer enters the indirect internal reformer guided by fuel feed plates and is reformed again by the aid of heat supplied from the bundles of tubular SOFCs through the reformer wall. During the reforming process, the exhaust gas from the indirect internal reformer contains mainly hydrogen and carbon monoxide together with a small quantity of un-reformed methane. The un-reformed methane with the other chemical components flowing into the SOFC module is reformed to hydrogen in the anode.

The air enters through a thin tube that is located centrally inside each tubular SOFC and is then made to flow back up to its open end. In general, approximately 80% of the supplied fuel (mainly hydrogen) is consumed by the electrochemical reaction in the fuel cell. This prevents possible fuel depletion from occurring near the fuel cell exit. Non-reacted fuel in the exhaust gas of the SOFC module, which is controlled by the fuel utilization factor, is burnt in the combustor.

Fuel and air streams along the longitudinal direction of the tubular SOFC participate in the electrochemical reaction to produce steam and the generation of electric power. The

temperatures of both streams are increased due to the exothermic electrochemical reaction. Some of the SOFC effluent in the depleted fuel plenum is recirculated to the inlet of the pre-reformer to provide necessary steam and heat for the reforming reaction. The amount of recirculated steam, denoted by the recirculation ratio, is an important design parameter that determines the system performance. On the other hand, the fuel stream in the depleted fuel plenum is oxidized in the combustor with the air stream at the exit of the bundles of tubular SOFCs. The high-temperature exhaust gas of the combustor is then supplied to the turbine to produce shaft power.

3. Mathematical models

3.1. Basic assumptions

For the performance analysis of the tubular SOFC/MGT hybrid power system described the above, it is necessary to develop mathematical models that govern the heat- and mass-transfer characteristics of each component of the system. For this purpose, some basic assumptions are made, as follows:

(i) the fuel supplied to the system is methane (CH_4);
(ii) the air supplied to the system is composed of 78.22% nitrogen (N_2), 20.74% oxygen (O_2), 0.03% carbon dioxide (CO_2), and 1.01% water (H_2O);
(iii) all chemical components of working fluids are treated as ideal gases;
(iv) the electrochemical reactions for both hydrogen (H_2) and carbon monoxide (CO) occur at the wall of each tubular SOFC;
(v) the operating cell voltage in each tubular SOFC is constant.

3.2. Quasi-2D model for SOFC module

Inside the SOFC bundle, fuel flows in a longitudinal direction along the outer surface, i.e., anode, of each tubular SOFC. Air is supplied into the tube located at the centre of each tubular SOFC. This air flows in a longitudinal direction through the annulus between the outside of the air-feed tube and the inner surface, i.e., cathode, of each tubular SOFC. The electrochemical reaction occurs in a radial direction in the three-layer wall, which is composed of the cathode (inner wall), electrolyte and anode (outer wall), of each tubular SOFC. This reaction is subject to the characteristics of mass transfer and also influences the characteristics of heat transfer. In this study, the model for mass- and heat-transfer analyses, the so-called the quasi-2D model, is conducted mainly in the flow direction, and takes taking into account the effects on the perpendicular directions related to the electrochemical reaction. Using this model, flow streams along the longitudinal direction of the indirect internal reformer and the tubular SOFC are divided into multiple segments, as shown in Fig. 2(a). Each segment is composed of several control volumes that are separated by walls between various flow streams. The chemical compositions and temperature at the exit of the control volume can be computed based on the mass and heat balances in each control volume. Chemical reaction processes, such as reforming and electrochemical reactions, contribute to the generation and/or consumption of chemical components in each control volume.

The fuel is reformed to hydrogen and carbon monoxide through steam reforming processes in the reformers and the anode of the SOFC. These processes involve two chemical reactions:

$$\text{fuel reforming}: \quad CH_4 + H_2O \leftrightarrow CO + 3H_2 \tag{1}$$

$$\text{steam shifting}: \quad CO + H_2O \leftrightarrow CO_2 + H_2 \tag{2}$$

The fuel reforming reaction is slow and highly endothermic, whereas, the steam shifting reaction is fast and weakly exothermic. Thus, the entire reforming process is dominated by the endothermic fuel reforming reaction that requires heat supplied from other sources. The steam shifting reaction is assumed to occur under chemical equilibrium conditions. This means that the steam shifting reaction occurs instantaneously and reaches equilibrium spontaneously. On the other hand, since the fuel reforming process is relatively slow, it is assumed that this reaction occurs at a finite rate. The reaction rate is very sensitive to the materials and catalysts used in the reformers and the anode of a SOFC. In this study, the model proposed by Achenbach [15] is adopted for the reaction rate of the fuel reforming reaction, namely:

$$\dot{r}_{CH_4} = k_{CH_4} p_{CH_4} \exp\left(\frac{-E_{CH_4}}{RT}\right) \tag{3}$$

Both hydrogen and carbon monoxide generated by the steam reforming process participate in the electrochemical reactions in SOFC, i.e.,

$$\text{hydrogen}: \quad H_2 + \frac{1}{2}O_2 \rightarrow H_2O \tag{4}$$

$$\text{carbon monoxide}: \quad CO + \frac{1}{2}O_2 \rightarrow CO_2 \tag{5}$$

The amounts of hydrogen and carbon monoxide consumed in the SOFC are directly related to the amount of generated electric power. The fuel utilization factor, U_f, defined as the ratio of consumed hydrogen and carbon monoxide to the amount of supplied fuel, is a parameter that represents the efficiency of the electrochemical reaction of the fuel cell, namely:

$$U_f \equiv \frac{z_{H_2} + z_{CO}}{4\dot{n}_{CH_4,\text{supplied}}} = \frac{(I/2F)}{4\dot{n}_{CH_4,\text{supplied}}} = \frac{jA}{8F\dot{n}_{CH_4,\text{supplied}}} \tag{6}$$

As shown in Eqs. (1) and (2), steam is a necessary participant in the reforming processes. It can be produced by

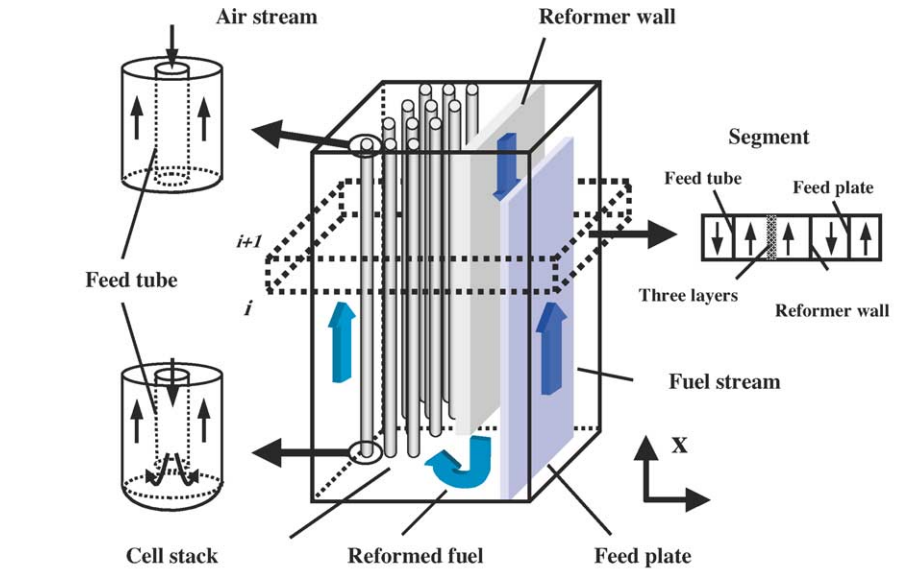

(a) Multiple segments along the longitudinal direction

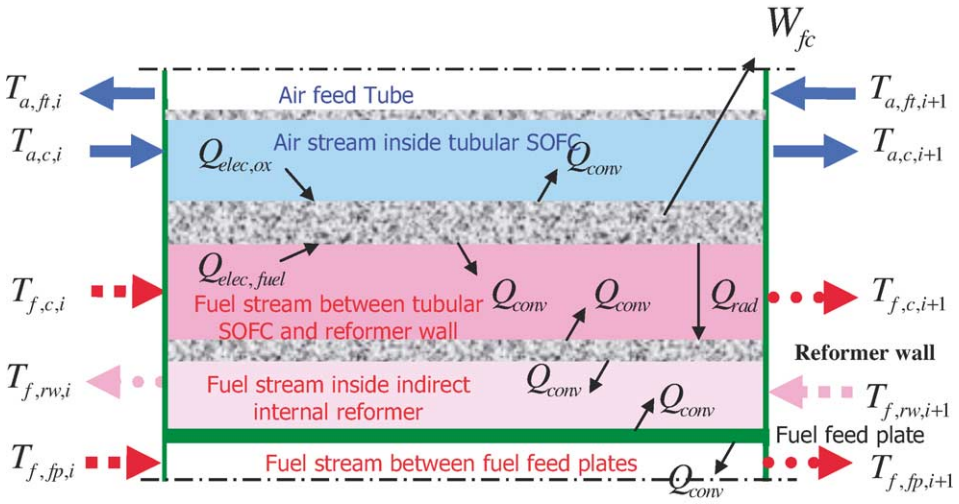

(b) Energy balances in control volumes in each segment

Fig. 2. Quasi-2D model for SOFC module: (a) multiple segments along longitudinal direction and (b) energy balances in control volumes in each segment.

the by-products of electrochemical reaction in the fuel cell. Therefore, the amount of recirculated exhaust gas, denoted as the recirculation ratio (RR) and defined as the ratio of the amount of recirculated gas to total amount of exhaust gas from the anode channel of the SOFC, is directly related to the steam–carbon ratio (SCR), which is defined as the ratio of steam to the supplied fuel. Thus:

$$\mathrm{RR} \equiv \left(\frac{\dot{n}_{\mathrm{CH_4,supplied}}}{\dot{n}_{\mathrm{H_2O,cell\,exit}}} \right) \mathrm{SCR} \tag{7}$$

Part of the heat generated by the electrochemical reaction in the tubular SOFC bundles is consumed by the direct reforming process that occurs simultaneously with the electrochemical reactions in the anode of the tubular SOFC, and part of the heat is transferred to the indirect internal reformer. The remainder is then used to raise the cell temperature. For heat-transfer analysis in flow streams that include the feed plate and the reformer wall, conduction in the solid walls, convection in the flow streams and radiation between tubular SOFCs and the reformer wall must all be taken into account, as illustrated in Fig. 2(b). Energy-balance equations governing the heat-transfer characteristics of control volumes in each segment of the quasi-2D model can be described as follows.

Inside air-feed tube

$$\sum \dot{n}_{x,i} \bar{h}_x(T_{\mathrm{a,ft},i}) - \sum \dot{n}_{x,i+1} \bar{h}_x(T_{\mathrm{a,ft},i+1}) = h_{\mathrm{a1}} A_{\mathrm{ft}} (T_{\mathrm{ft},i} - T_{\mathrm{a,ft},m}) \tag{8}$$

where the right-hand side is the convective heat-transfer rate between the inner wall of the air-feed tube and the air-flow

stream; $\dot{n}_{x,i}$ represents the molar flow rate of x species at the ith segment.

Between air-feed tube and inner wall of tubular SOFC

$$\sum \dot{n}_{x,i+1}\bar{h}_x(T_{\mathrm{a,c},i+1}) - \sum \dot{n}_{x,i}\bar{h}_x(T_{\mathrm{a,c},i}) = h_{\mathrm{a2}}A_{\mathrm{c}}(T_{\mathrm{c},i} - T_{\mathrm{a,c},m}) + h_{\mathrm{a3}}A_{\mathrm{ft}}(T_{\mathrm{ft},i} - T_{\mathrm{a,c},m}) - \dot{Q}_{\mathrm{elec,ox}} \quad (9)$$

with

$$\dot{Q}_{\mathrm{elec,ox}} = \frac{1}{2}(z_{\mathrm{H_2}} + z_{\mathrm{CO}})\bar{h}_{\mathrm{O_2}}(T_{\mathrm{a,c},m}) \quad (10)$$

representing the heat transfer caused by the consumption of oxygen for the electrochemical reaction in the tubular SOFC wall. The first two terms of the right-hand side in Eq. (9) are the convective heat-transfer rates between the air flow stream inside the annulus and the tube walls, e.g., SOFC tube and air-feed tube, respectively.

At wall of air-feed tube

$$h_{\mathrm{a1}}A_{\mathrm{c}}(T_{\mathrm{ft},i} - T_{\mathrm{a,ft},m}) + h_{\mathrm{a3}}A_{\mathrm{ft}}(T_{\mathrm{ft},i} - T_{\mathrm{a,c},m}) = 0 \quad (11)$$

With the assumption of a thin air-feed tube, heat conduction is not considered in this case.

Between outer wall of tubular SOFC and reformer wall

$$\sum \dot{n}_{x,i+1}\bar{h}_x(T_{\mathrm{f,c},i+1}) - \sum \dot{n}_{x,i}\bar{h}_x(T_{\mathrm{f,c},i}) = h_{\mathrm{f1}}A_{\mathrm{c}}(T_{\mathrm{c},i} - T_{\mathrm{f,c},m}) + h_{\mathrm{f2}}A_{\mathrm{rw}}(T_{\mathrm{rw},i} - T_{\mathrm{f,c},m}) - \dot{Q}_{\mathrm{elec,fuel}} \quad (12)$$

with

$$\dot{Q}_{\mathrm{elec,fuel}} = z_{\mathrm{H_2}}[\bar{h}_{\mathrm{H_2}}(T_{\mathrm{f,c},m}) - \bar{h}_{\mathrm{H_2O}}(T_{\mathrm{c},i})] + z_{\mathrm{CO}}[\bar{h}_{\mathrm{CO}}(T_{\mathrm{f,c},m}) - \bar{h}_{\mathrm{CO_2}}(T_{\mathrm{c},i})] \quad (13)$$

representing the heat transfer caused by the consumption of hydrogen and carbon monoxide and by the generation of steam and carbon dioxide in the electrochemical reaction in the tubular SOFC.

At wall of tubular SOFC:

$$\dot{Q}_{\mathrm{elec,fuel}} + \dot{Q}_{\mathrm{elec,ox}} - \dot{W}_{\mathrm{FC},i} = h_{\mathrm{a2}}A_{\mathrm{c}}(T_{\mathrm{c},i} - T_{\mathrm{a,c},m}) + h_{\mathrm{f1}}A_{\mathrm{c}}(T_{\mathrm{c},i} - T_{\mathrm{f,c},m}) + \dot{Q}_{\mathrm{rad}} - k_{\mathrm{s,c}}A_{\mathrm{s,c}}\Delta x\frac{\mathrm{d}^2T_{\mathrm{c}}}{\mathrm{d}x^2} \quad (14)$$

with

$$\dot{Q}_{\mathrm{rad}} = \sigma A_{\mathrm{rad}}\sum_{j=1}^{N}\frac{(T_{\mathrm{c},i}^4 - T_{\mathrm{rw},j}^4)}{\frac{1-\varepsilon_{\mathrm{c}}}{\varepsilon_{\mathrm{c}}} + \frac{1}{F_{i-j}} + \frac{1-\varepsilon_{\mathrm{rw}}}{\varepsilon_{\mathrm{rw}}}} \quad (15)$$

representing the radiative heat transfer rate between the ith segment of the SOFC wall and the reformer wall. The last term of the right-hand side in Eq. (14) represents the heat conduction rate inside wall of the tubular SOFC in a longitudinal direction. The first two terms of the right-hand side represents the convective heat transfer with air and fuel flow streams, respectively.

Between fuel-feed plates

$$\sum \dot{n}_{x,i+1}\bar{h}(T_{\mathrm{f,fp},i+1}) - \sum \dot{n}_{x,i}\bar{h}(T_{\mathrm{f,fp},i}) = h_{\mathrm{fp}}A_{\mathrm{fp}}(T_{\mathrm{fp},i} - T_{\mathrm{f,fp},m}) \quad (16)$$

where the right-hand side is the convective heat transfer between the fuel stream and the fuel-feed plates.

Between fuel-feed plate and reforming wall:

$$\sum \dot{n}_{x,i}\bar{h}_x(T_{\mathrm{f,rw},i}) - \sum \dot{n}_{x,i+1}\bar{h}_x(T_{\mathrm{f,rw},i+1}) = h_{\mathrm{r1}}A_{\mathrm{rw}}(T_{\mathrm{rw},i} - T_{\mathrm{f,rw},m}) + h_{\mathrm{r2}}A_{\mathrm{fp}}(T_{\mathrm{fp},i} - T_{\mathrm{f,rw},m}) \quad (17)$$

where two terms on the right-hand side represent convective heat-transfer rates between the fuel stream and the surrounding walls.

At the fuel-feed plate

$$h_{\mathrm{r2}}A_{\mathrm{fp}}(T_{\mathrm{fp},i} - T_{\mathrm{f,rw},m}) + h_{\mathrm{fp}}A_{\mathrm{fp}}(T_{\mathrm{fp},i} - T_{\mathrm{f,fp},m}) = 0 \quad (18)$$

As denoted in case of the air-feed tube, fuel-feed plates are also assumed to be very thin so that the conduction effect is negligible.

At the reforming wall

$$\dot{Q}_{\mathrm{rad}} = h_{\mathrm{f2}}A_{\mathrm{rw}}(T_{\mathrm{rw},i} - T_{\mathrm{f,c},m}) + h_{\mathrm{r1}}A_{\mathrm{rw}}(T_{\mathrm{rw},i} - T_{\mathrm{f,rw},m}) - k_{\mathrm{s,rw}}A_{\mathrm{s,rw}}\,\Delta x\frac{\mathrm{d}^2T_{\mathrm{rw}}}{\mathrm{d}x^2} \quad (19)$$

with

$$\dot{Q}_{\mathrm{rad}} = \sigma A_{\mathrm{rad}}\sum_{j=1}^{N}\frac{(T_{\mathrm{c},j}^4 - T_{\mathrm{rw},i}^4)}{\frac{1-\varepsilon_{\mathrm{c}}}{\varepsilon_{\mathrm{c}}} + \frac{1}{F_{i-j}} + \frac{1-\varepsilon_{\mathrm{rw}}}{\varepsilon_{\mathrm{rw}}}} \quad (20)$$

representing the radiative heat-transfer rate between the ith segment of the reformer wall and the SOFC wall. The last term of the right-hand side in Eq. (19) represents the conductive heat-transfer rate inside the reformer wall along a longitudinal direction. The first two terms of the right-hand side in Eq. (19) represents heat convection with two fuel flow streams around the reformer wall.

3.3. Lumped model for MGT system

The micro gas turbine adopted for the tubular SOFC/MGT hybrid power system is composed of four major components, namely: compressor, combustor, turbine, and recuperator. Since the compressor and turbine in the MGT are generally single-stage centrifugal and radial types, respectively, the lumped model can be applied. By considering energy balances in compressor and turbine with known inlet conditions, the exit conditions can be easily computed with the functions of isentropic efficiencies. In the present study, it is assumed that the turbine inlet temperature (TIT) of the MGT is fixed during operation of the system. The role of the combustor is to

burn the effluent gas of the SOFC, which contains hydrogen, carbon monoxide and methane, and to raise the exit temperature to the TIT. The chemical reactions in the combustor are:

$$\text{hydrogen}: \quad H_2 + \frac{1}{2}O_2 \rightarrow H_2O \tag{21}$$

$$\text{carbon monoxide}: \quad CO + \frac{1}{2}O_2 \rightarrow CO_2 \tag{22}$$

$$\text{methane}: \quad CH_4 + 2O_2 \rightarrow CO_2 + 2H_2O \tag{23}$$

By applying a lumped model to the combustor, the compositions of the chemical components of the combustor exhaust gas and its temperature can be computed based on mass and energy balance equations. The recuperator preheats compressed air before entering the pre-reformer through the high temperature of the exhaust gas of the turbine. Therefore, the air temperature entering the pre-reformer can be expressed as a function of the heat-exchange effectiveness of the recuperator and the temperatures of entering streams to the recuperator.

3.4. System performance

The maximum available power that can be produced by the electrochemical reaction in the fuel cell is the difference in the Gibbs free energy between the products and reactants of the reaction that can be converted to the open-circuit voltage as follows:

$$\begin{aligned}\dot{W}_{\text{FC max}} &= -\Delta\dot{G} = -(z_{H_2} + z_{CO})\Delta\bar{g} \\ &= 2(z_{H_2} + z_{CO})FV_{oc}\end{aligned} \tag{24}$$

Since the chemical components are considered to be ideal gases, the difference in the Gibbs free energy per one mole of hydrogen can be expressed as:

$$-\Delta\bar{g} = -\Delta\bar{g}^0 + RT\ \ln\left[\frac{P_{H_2}/P_0(P_{O_2}/P_0)^{1/2}}{P_{H_2O}/P_0}\right] \tag{25}$$

The difference of Gibbs free energy per one mole of carbon monoxide is equal to that of hydrogen [15]. This means that the open-circuit voltages of hydrogen and carbon monoxide have the same value.

By defining the current density, j, as the rate of electron transfer per unit activation area of the fuel cell, the electric power produced by the fuel cell can be expressed by:

$$\dot{W}_{FC} = V_c j A_c \tag{26}$$

The cell voltage is the difference between open-circuit voltage and voltage losses in the fuel cell, i.e.,

$$V_c = V_{oc} - \Delta V_{loss} \tag{27}$$

where ΔV_{loss} is the sum of the voltage losses due to irreversibilities in the fuel cell that include activation polarization, ohmic losses, concentration loss, etc. At the high-operating temperature of the SOFC, the concentration loss can be ignored because the diffusion is a very efficient process [16,17]. In the present study, only the activation polarization and ohmic losses have been taken into consideration:

$$\Delta V_{loss} = \Delta V_{act} + \Delta V_{ohm} \tag{28}$$

where ΔV_{act} is the activation polarization and ΔV_{ohm} is the ohmic loss. The empirical equations by Achenbach [15] are adopted for the activation polarization. The ohmic losses in the tubular SOFC are considered not only with current flow in the radial direction, but also with circumferential current flow through the anode and cathode. Detailed mathematical deviations of the ohmic losses are described in Appendix A.

The efficiencies of the SOFC and related SOFC/MGT hybrid power system are defined, respectively, as follows:

$$\eta_{FC} = \frac{\dot{W}_{FC}}{\dot{m}_{CH_4}(\text{LHV})_{CH_4}} \tag{29}$$

$$\eta_{SYS} = \frac{\dot{W}_{FC} + \dot{W}_{GT}}{\dot{m}_{CH_4}(\text{LHV})_{CH_4}} \tag{30}$$

4. Results and discussions

The mathematical formulations discussed in the previous section were applied to the performance analysis of a tubular SOFC/MGT hybrid power system. Most of the reference data used in this study (Table 1) are based on published data of Siemens–Westinghouse products [7,18,19]. Some of those values, including compressor and turbine efficiencies, were assumed by their up-to-date general performance trends.

The purpose of the above work is to investigate the influence of system characteristics on the design-point performance of the system. Here, the design-point performance means that all components in the hybrid system are operated with their design-point condition. Therefore, the off-design performance with different operating conditions from the design-point performance has been excluded from the scope of this study.

To investigate the influence of the component characteristics on the hybrid system clearly, the total produced power of the system was fixed. Under such a condition, the impact of different values of the parameters on the performance of both the SOFC and the MGT can be clearly determined. Also, it is assumed that the hybrid system is operated with a fixed turbine inlet temperature. Details of the computational procedures are described elsewhere [20].

4.1. Feasibility of quasi-2D model

The computational accuracy of the quasi-2D model depends on the appropriate choice of the number of segments along the longitudinal direction of the tubular SOFC. As shown in Fig. 3, the distributions of cell temperature and

Table 1
Reference data for performance analysis (quoted from Siemens–Westinghouse [7,18,19])

Parameter	Value
Physical conditions	
System	
Ambient conditions (°C, atm)	15, 1
System power (kW)	220
Fuel cell	
Steam–carbon ratio	2.5
Fuel utilization factor	0.85
Average current density (A m^{-2})	3200
Fuel inlet temperature (°C)	15
Gas turbine	
Pressure ratio	2.9
Turbine inlet temperature (°C)	840
Compressor adiabatic efficiency (%)	78
Turbine adiabatic efficiency (%)	82
Recuperator effectiveness (%)	89
Geometry of tubular SOFC	
Cathode thickness (mm)	2
Electrolyte thickness (μm)	40
Anode thickness (μm)	125
Interconnector thickness (μm)	100
Interconnector width (cm)	0.9
Numerical conditions	
Number of segments along longitudinal direction of the tubular IIR-SOFC system	

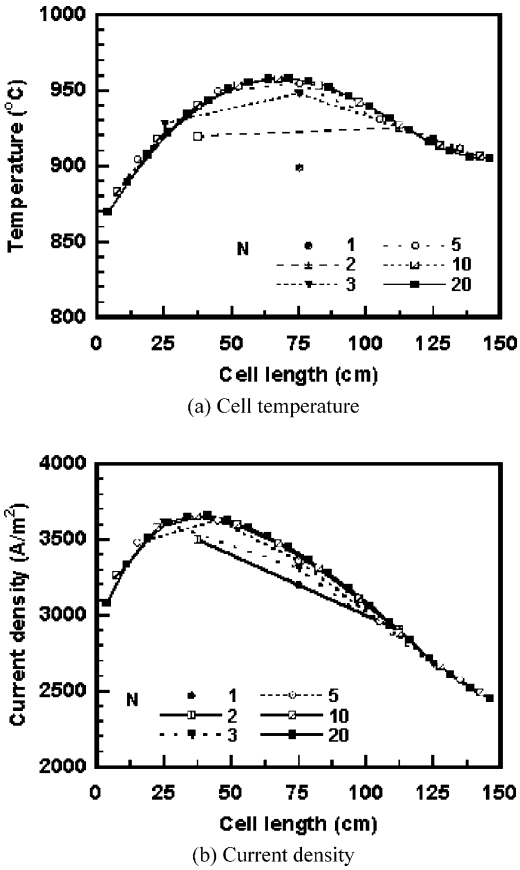

(a) Cell temperature

(b) Current density

Fig. 3. Distributions of cell temperature and current density along longitudinal direction of tubular SOFC with different number of segments: (a) cell temperature and (b) current density.

current density along the longitudinal direction of the tubular SOFC converge to form specific patterns as the number of segments increases. It is noted that the mean value of the converged cell temperature in the quasi-2D model (929.40 °C) is much higher than the value calculated by the lumped model (899.90 °C). The latter is the same as that when the number of segments is one in the quasi-2D model. In addition, it can be seen that there exists a considerable temperature difference along the length (74.12 °C) of the SOFC that cannot be predicted by the lumped model. This value can be used to assess the thermo-mechanical strength of the SOFC. Also, Table 2 shows that some important parameters related to the performance of the hybrid system converge as the number of segments increases.

4.2. Different characteristics of system components

As shown by the data in Figs. 1 and 2, the SOFC module of the hybrid system considered in this study is composed of many components, namely: bundles of tubular SOFCs, a pre-reformer, an indirect internal reformer, and a combustor. The performance characteristics of the SOFC and also the entire hybrid system are greatly dependent on the configurations of the components and their arrangements within the system. For example, the directions in which the air and the fuel streams flow in the tubular SOFC influences the characteristics of heat and mass transfer, the electrochemical reaction and, consequently, the fuel cell performance. Thus, in order to provide adequate directions, it is important that the various components in the SOFC module are properly arranged. Also, as described in previous sections, in spite of the direct internal reforming capability in the anode of the SOFC, reforming reactions at either the pre-reformer or the internal reformer prior to the SOFC are essential. Therefore, it is also necessary to investigate the impact of the characteristics of these reformers on the performance and operating characteristics of the hybrid system.

4.2.1. Different flow paths of supplied fuel to SOFC

Two different structures of the SOFC module, as shown in Fig. 4, have been considered to investigate the influence of directions of flow streams along the tubular SOFC. The same case as the original one described in Fig. 2 is shown in Fig. 4(a). This case, which is the so-called co-flow condition, can be seen to flow in the same direction as the air and fuel streams along the wall of the tubular SOFC. For the counter-flow case (Fig. 4(b)), the direction of the fuel stream along the outer wall of the tubular SOFC is seen to show an opposing trend to the co-flow case (Fig. 4(a)). Different directions of the fuel stream along the outer wall of the tubular SOFC are similarly applied to those in the fuel feed and the internal reforming streams.

Table 2
Computational results of system performance with different number of segments along longitudinal direction of SOFC module

Parameter	Siemens–Westinghouse [7]	Number of segments			
		$N=1$	$N=5$	$N=10$	$N=20$
Current density ($A\,m^{-2}$)	3200	**3200**	**3200**	**3200**	**3200**
Cell operating voltage (V)	0.610	0.540	0.607	0.611	0.613
Pressure ratio	2.9	**2.9**	**2.9**	**2.9**	**2.9**
Air mass flow rate ($kg\,s^{-1}$)	0.5897	0.7128	0.5964	0.5898	0.5867
TIT (°C)	840	**840**	**840**	**840**	**840**
SOFG dc power (kW)	187	175.0	184.3	184.7	185.0
SOFG ac power (kW)	176	166.4	175.0	175.5	175.7
GT ac power (kW)	47	55.4	46.7	46.2	45.9
Net ac power (kW)	220	**220**	**220**	**220**	**220**
System efficiency (%)	57	56.0	59.8	60.1	60.2
Cell active area (m^2)	96	101.3	94.9	94.5	94.3

Bold characters are given values.

In both cases, the temperatures of both the air and the fuel streams along the tubular SOFC increase on their entry into the SOFC due to the exothermic electrochemical reaction, and to decrease in the downstream region of the SOFC due to the heat transferred from the SOFC to the indirect internal reformer. A comparison of the temperature distributions in the flow streams in both the co-flow and the counter-flow cases is presented in Fig. 5. It can be seen that the temperature of the fuel stream on entering the SOFC in the counter-flow case falls earlier than the co-flow case. This is because the region of low temperature near the bottom of the SOFC reduces the amount of heat required for the reforming process in the indirect internal reformer. This could cause a delay in the reforming process in the indirect internal reformer. As shown in Fig. 6, the cell temperature of the counter-flow case has a peak value near the entrance, i.e., the top of the SOFC, and is lower than that of the co-flow case at the bottom of the SOFC. This causes the maximum difference in the cell temperature along the SOFC in the counter-flow case (144.25 °C) to become almost double compared with the other case (72.12 °C). On the other hand, the mean cell temperature of the counter-flow case (903.41 °C) is lower than the co-flow case (929.40 °C).

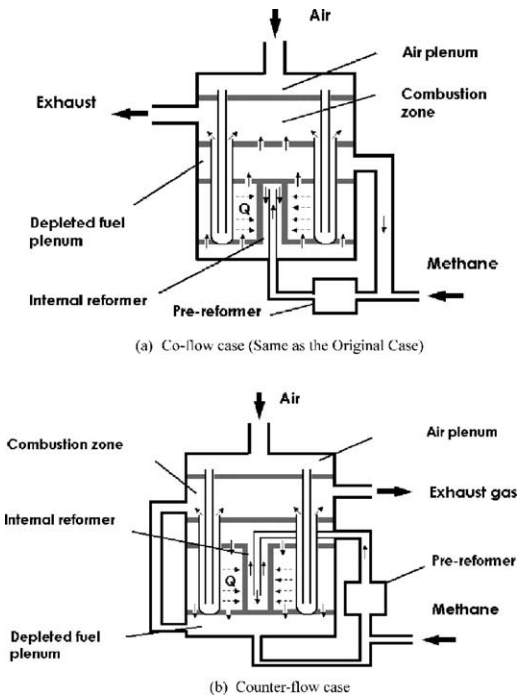

Fig. 4. Schematic diagrams for different directions of fuel streams in SOFC module: (a) co-flow case (same as original case) and (b) counter-flow case.

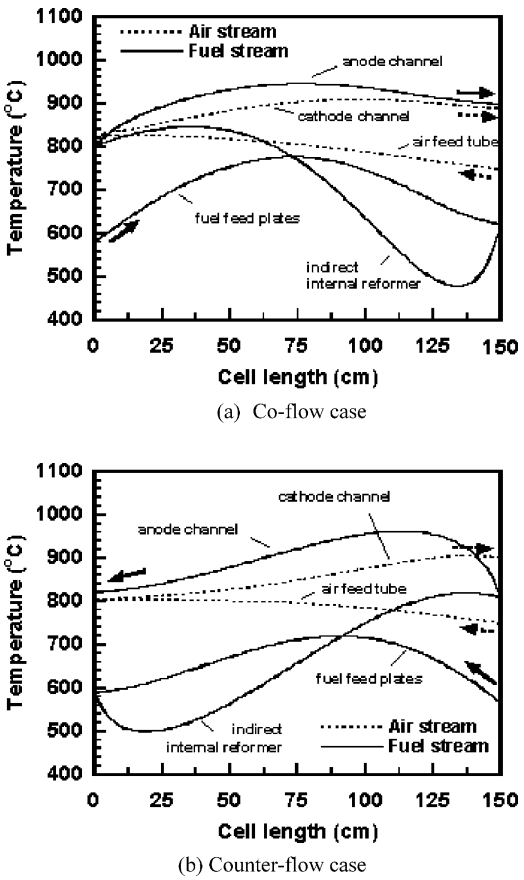

Fig. 5. Temperature distributions in SOFC module with different directions of fuel streams along longitudinal direction of tubular SOFC: (a) co-flow case (same as original case) and (b) counter-flow case.

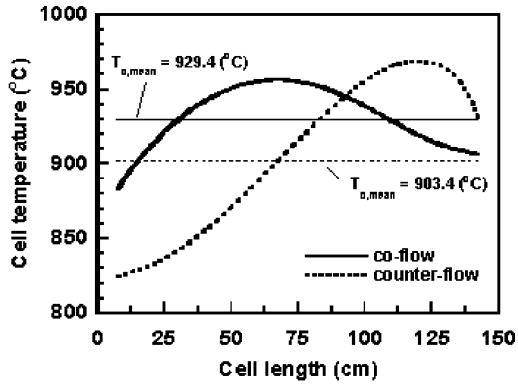

(a) Cell temperature

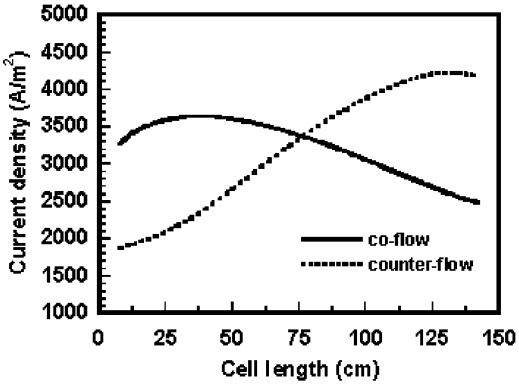

(b) Current density

Fig. 6. Distributions of cell temperature and current density along longitudinal direction of tubular SOFC with different directions of fuel streams in SOFC module: (a) cell temperature and (b) current density.

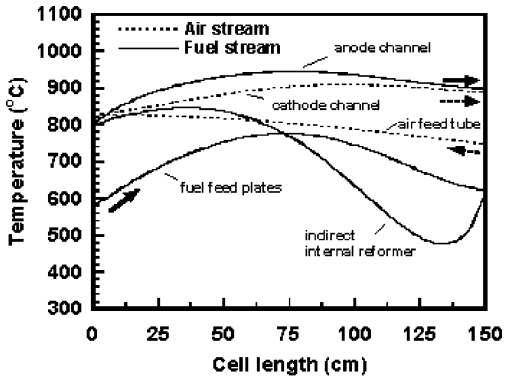

(a) With a pre-reformer,

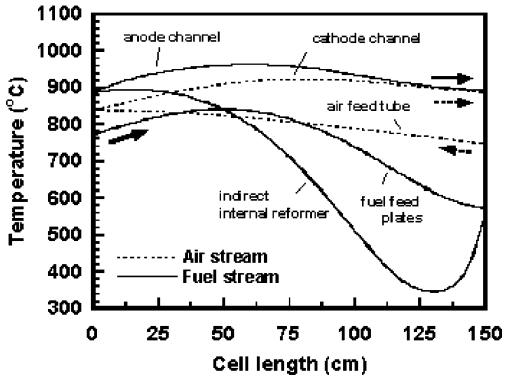

(b) Without a pre-reformer

Fig. 7. Temperature distributions along flow streams in SOFC module: (a) with pre-reformer (same as original case) and (b) without pre-reformer.

The distributions of current density are very similar to those of cell temperature.

The low mean cell temperature of the counter-flow case may reduce the cell voltage and the fuel cell efficiency, but its influence is not very significant, as shown in Table 3. For the hybrid system, however, because of the reduction, in the power generated by the fuel cell (high-efficiency module) due to the low cell temperature and the increase in gas turbine (low efficiency module) power to meet the required total power, the reduction in efficiency is dominant in the counter-flow case.

4.2.2. Existence of a pre-reformer

A pre-reformer, located at the front of the indirect internal reformer, as shown in Fig. 1, converts supplied fuel (methane) to hydrogen and carbon monoxide by the steam-reforming reaction. The steam and heat is supplied by the recirculated exhaust gas stream from the anode of the SOFC. The role of the pre-reformer to reduce the reforming load of the indirect reforming processes in both the indirect internal reformer itself and the anode of the SOFC. To investigate the influence of a pre-reformer on the system performance, analyses were conducted with and without a pre-reformer and the respective results were compared.

Table 3
Comparisons of system performance with different flow directions along the longitudinal direction of SOFC module

Case	Co-flow	Counter-flow
Cell voltage (V)	0.611	0.584
η_{FC} (%)	47.9	47.6
W_{FC}/W_{GT}	3.80	3.47
η_{SYS} (%)	60.1	57.7

As shown in Fig. 7, when a pre-reformer is eliminated, the temperature of the fuel stream entering between the fuel-feed plates is higher than in the case with a pre-reformer. This is due to the heat-absorbing process in the pre-reformer. The high-temperature fuel stream when not using a pre-reformer also increases the cell temperature (Fig. 8(a)). The mean cell temperatures with and without a pre-reformer are 929.40 and 943.00 °C, respectively. The maximum differences in the cell temperature along the SOFC length in the two cases are almost the same, i.e., 74.12 °C with a pre-reformer and 72.41 °C without a pre-reformer. As shown in Table 4, the high-cell temperature without a pre-reformer assists the rise in the cell voltage and thereby to improve the efficiency of the fuel cell. As a result, it contributes to the enhancement of the efficiency of the hybrid system mainly through an increase in fuel cell power. On the other hand, the pre-reformer

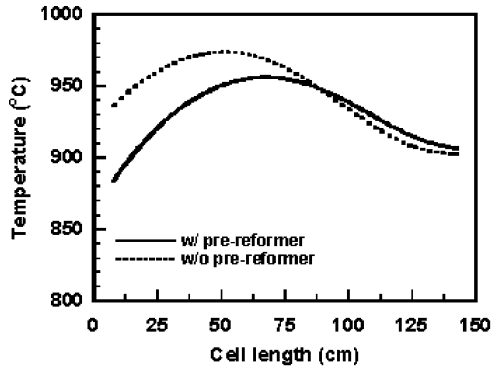

(a) Cell temperature

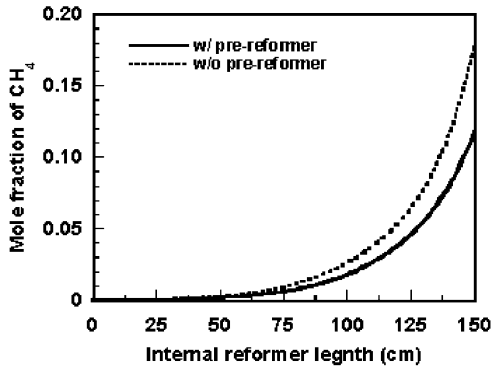

(b) Amount of methane in the indirect internal reformer

Fig. 8. Influence of pre-reformer on cell temperature and amount of methane in indirect internal reformer: (a) cell temperature and (b) amount of methane in indirect internal reformer.

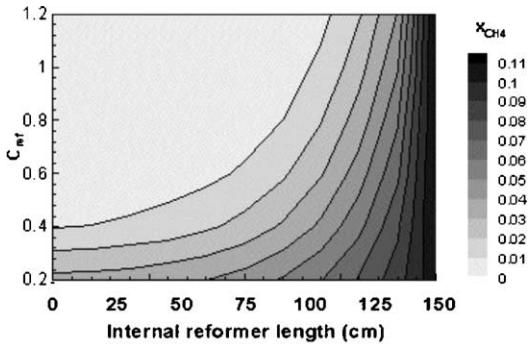

(a) Distributions of the amount of methane

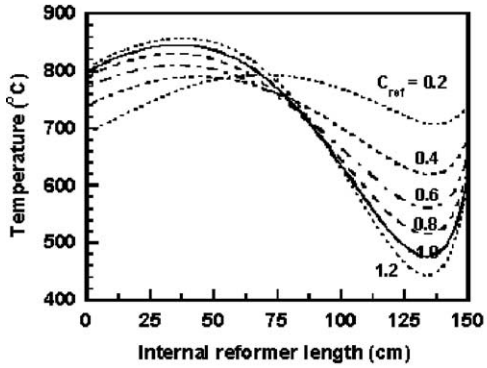

(b) Distributions of temperature of the reformer wall

Fig. 9. Influence of catalyst density of indirect internal reformer on mass and heat transfer characteristics in indirect internal reformer: (a) distributions of amount of methane and (b) distribution of temperature of reformer wall.

is a very helpful device in that it relaxes the reforming load of the indirect internal reformer. In addition, it reduces the amount of methane that enters the flow channel of the SOFC and thus reduces the possibility of carbon deposition at the anode.

4.2.3. Catalyst density of indirect internal reformer

In this study, more than 99% of the supplied methane was reformed to hydrogen and carbon monoxide in both the pre-reformer and the indirect internal reformer. As the performance analysis showed that 25–30% of the supplied methane was reformed by the pre-reformer, it can easily be concluded that the indirect internal reformer that processes the remaining methane plays a very important role. The capability of a reformer depends on the amount of the catalyst. To investigate the influence of the reforming capability of the indirect internal reformer on the system performance, the reforming reaction expressed by Eq. (3) is revised as follows:

$$\dot{r}_{CH_4} = C_{ref} k_{CH_4} p_{CH_4} \exp\left(\frac{-E_{CH_4}}{RT}\right) \quad (31)$$

Here, C_{ref} can be treated as a parameter that governs the amount of the reforming reaction in the indirect internal reformer and, therefore, it is assumed that the catalyst density is proportional to this value. A high C_{ref} value represents a high-catalyst density.

As shown in Fig. 9, C_{ref} influences the distribution of methane and the temperature of the fuel stream along the longitudinal direction of the indirect internal reformer. In addition, it can be seen that the reforming reaction occurs as soon as methane enters the indirect internal reformer and is concentrated near the entrance at a high-catalyst density. Furthermore, due to the endothermic characteristics of the reforming reaction, the temperature of the fuel stream falls sharply in the same region where the reforming reaction is dominant.

The catalyst density is also strongly related to the distributions of the cell temperature and the current density, as illustrated in Fig. 10. The difference in cell temperature along the longitudinal direction of the SOFC becomes large at a low catalyst density. As demonstrated in Table 5, a high-catalyst density in the indirect internal reformer causes an improvement in the performance of the SOFC and, consequently, to the performance of the related hybrid system. It should be

Table 4
Influence of existence of a pre-reformer on system performance

Case	With a pre-reformer	Without a pre-reformer
Cell voltage (V)	0.611	0.620
η_{FC} (%)	47.9	48.7
W_{FC}/W_{GT}	3.80	3.93
η_{SYS} (%)	60.1	60.6

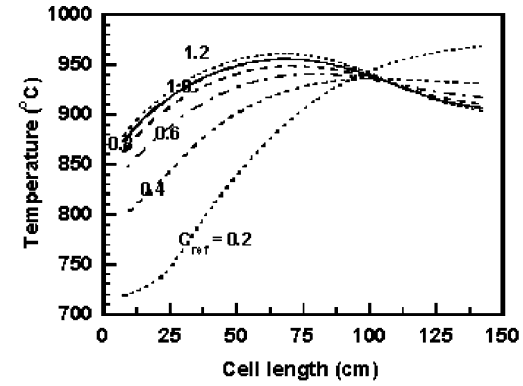

(a) Cell temperature

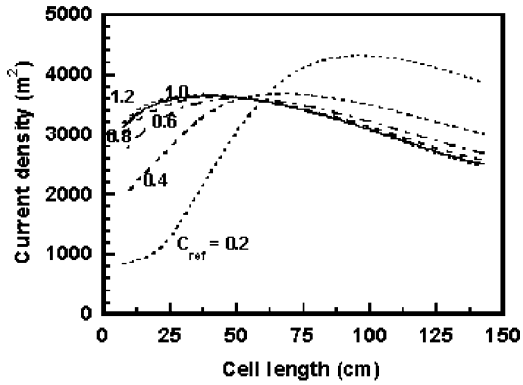

(b) Current density

Fig. 10. Influence of catalyst density of indirect internal reformer on distributions of cell temperature and current density along longitudinal direction of tubular SOFC: (a) cell temperature and (b) current density.

Table 5
Influence of catalyst density of indirect internal reformer on system performance

Case	C_{ref}			
	0.2	0.6	1.0	1.2
Cell voltage (V)	0.527	0.600	0.611	0.613
η_{FC} (%)	41.4	47.1	47.9	48.1
W_{FC}/W_{GT}	2.88	3.67	3.80	3.81
η_{SYS} (%)	55.3	59.5	60.1	60.1

noted that a low catalyst density gives rise to a significant deterioration in system performance.

5. Conclusions

A quasi-2D model has been introduced and takes into account the heat and mass transfer characteristics of tubular SOFCs and related reforming processes. Performance analysis of a tubular SOFC/MGT hybrid power system has been conducted based on this quasi-2D model. The model makes it possible to predict the temperatures of the fuel and the air flow streams along the longitudinal direction of a SOFC module that is composed of bundles of tubular SOFCs and an indirect internal reformer. Feasibility studies for the quasi-2D model prove that the computational results converged to certain values and/or patterns with increase in the number of segments along the longitudinal direction of the SOFC module.

Different flow directions of the fuel streams outside of tubular SOFCs showed different patterns of cell temperatures along the longitudinal direction and are found to influence the performance of the system itself. It is expected that the co-flow case will provide a high mean cell temperature, which in turn, will enhance the system performance compared with the counter-flow alternative. If a pre-reformer, located prior to the indirect internal reformer, is eliminated then the cell temperature will increase. It is found that the pre-reformer plays an important role in reducing the load of the indirect internal reformer. Finally, it is shown that the catalytic density of the indirect internal reformer influences significantly the system performance.

Appendix A. Loss Models in a Tubular SOFC

Activation polarization is caused by the slowness of the electrochemical reactions taking place on the surface of electrodes. It is very non-linear and difficult to express analytically. The model for activation polarization used in this study is adopted from Achenbach [15], i.e.,

$$\Delta V_{act} = \Delta V_{act,a} + \Delta V_{act,c} = j r_c + j_{H_2} r_{a,H_2} \tag{A.1}$$

with

$$\frac{1}{r_c} = \frac{4F}{RT} k_c \left(\frac{p_{O_2}}{P_0}\right)^m \exp\left(-\frac{E_c}{RT}\right) \tag{A.2}$$

$$\frac{1}{r_{a,H_2}} = \frac{2F}{RT} k_{a,H_2} \left(\frac{p_{H_2}}{P_0}\right)^m \exp\left(\frac{-E_a}{RT}\right) \tag{A.3}$$

where r represents the area specific electrical resistance. The influence of partial pressure on the losses is accounted by the slope of $m = 0.25$. The activation energy of the cathode and anode is set to $E_{ca} = 160\,\mathrm{kJ\,mol^{-1}}$ and $E_{an} = 110\,\mathrm{kJ\,mol^{-1}}$, respectively. The pre-exponential factors are given as $k_{ca} = 1.49 \times 1010\,\mathrm{A\,m^{-2}}$ and $k_{an,H_2} = 2.13 \times 108\,\mathrm{A\,m^{-2}}$.

Ohmic losses occur due to the electrical resistance to the flow of electrons or ionic species. Fig. A1 shows the paths of (i) the electrons through the cathode, (ii) the oxygen ions through the electrolyte, and (iii) the electrons through the anode in a tubular SOFC. In this study, an ohmic loss model taking into account realistic electron/ion paths is developed based on Tanaka et al. [21]. It is assumed that the electron flux at the entrance of the cathode or at the exit of the anode is uniform in the circumferential direction, and that an uniform ionic flux penetrates the entire electrolyte. In Fig. 3, angles $A\pi$ and $B\pi$ are related to the extent of electrical contact on the half of the cell tube and the interconnector, respectively. The final forms of the ohmic losses in a tubular SOFC are represented as follows for the anode, cathode, electrolyte and

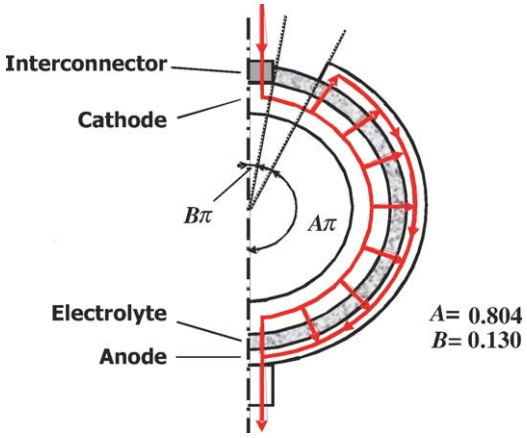

Fig. A1. Electronic/ionic flows in tubular SOFC.

interconnector, respectively:

$$\Delta V_{\mathrm{ohm,a}} = \frac{\sigma\rho_{\mathrm{a}}(A\pi D)^2}{8d_{\mathrm{a}}} \tag{A.4}$$

$$\Delta V_{\mathrm{ohm,c}} = \frac{\sigma\rho_{\mathrm{c}}(\pi D)^2}{8d_{\mathrm{c}}} A[A + 2(1 - A - B)] \tag{A.5}$$

$$\Delta V_{\mathrm{ohm,e}} = j\rho_{\mathrm{e}}d_{\mathrm{e}} \tag{A.6}$$

$$\Delta V_{\mathrm{ohm,int}} = j(\pi D)\rho_{\mathrm{int}}\frac{d_{\mathrm{int}}}{w_{\mathrm{int}}} \tag{A.7}$$

where ρ_i and d_i, are the resistivity and thickness of component i, D the mean diameter of the tubular SOFC, and w_{int} the width of the interconnector. The resistivity of each layer of SOFC is treated as a function of the local operating temperature [22].

References

[1] J. Larminie, A. Dicks, Fuel Cell System Explained, John Wiley & Sons Ltd., New York, 2000.
[2] S.P. Harvey, H.J. Richter, Gas turbine cycles with solid oxide fuel cells. Part I: Improved gas turbine power plant efficiency by use of recycled exhaust gases and fuel cell technology, Trans. ASME: J. Energy Resour. Technol. 116 (1994) 305–311.
[3] S. Campanari, Full-load and part-load performance prediction for integrated SOFC and microturbine systems, Trans. ASME: J. Eng. Gas Turbines Power 122 (2000) 239–246.
[4] S. Freni, M. Aquino, E. Passalacqua, Molten carbonate fuel cell with indirect internal reforming, J. Power Sources 52 (1994) 41–47.
[5] A.F. Massardo, F. Lubelli, Internal reforming solid oxide fuel cell-gas turbine combined cycles (IRSOFC-GT). Part A: Cell model and cycle thermodynamic analysis, Trans. ASME: J. Eng. Gas Turbines Power 122 (2000) 27–35.
[6] S.E. Veyo, L.A. Shockling, J.T. Dederer, J.E. Gillett, W.L. Lundberg, Tubular solid oxide fuel cell/gas turbine hybrid cycle power systems: status, Trans. ASME: J. Eng. Gas Turbines Power 124 (2002) 845–849.
[7] R.A. George, Status of tubular SOFC field unit demonstrations, J. Power Sources 86 (2000) 134–139.
[8] W.L. Lundberg, S.E. Veyo, A high-efficiency SOFC hybrid power system using the mercury 50 ATS gas turbine, ASME Paper GT2001-0521, 2001.
[9] S.E. Veyo, K.P. Litzinger, S.D. Vora, W.L. Lundberg, Status of pressurized SOFC/gas turbine power system development at Siemens Westinghouse, ASME Paper GT2002-30670, 2002.
[10] S.E. Veyo, W.L. Lundberg, K.P. Litzinger, Tubular SOFC hybrid power system status, ASME Paper GT2003-38943, 2003.
[11] J.H. Kim, K. Suzuki, Performance analysis of SOFC/MGT hybrid system, Proc. KSME Spring Annu. Meet. B (2001) 703–707.
[12] T.W. Song, J.H. Kim, S.T. Ro, K. Suzuki, Multi-Stage model for indirect internal reforming type solid oxide fuel cells, Proc. Int. Conf. Power Eng. 03 2 (2003) 433–438.
[13] F. Bevc, Advances in solid oxide fuel cells and integrated power plants, Proc. Institute Mech. Eng., Part A: J. Power Energy 211 (1997) 359–366.
[14] R.A. George, N.F. Bessette, Reducing the manufacturing cost of tubular SOFC technology, J. Power Sources 86 (1998) 131–137.
[15] E. Achenbach, Three-dimensional and time-dependent simulation of a planar solid oxide fuel cell stack, J. Power Sources 49 (1994) 333–348.
[16] P. Costamagna, L. Magistri, A.F. Massardo, Design and part-load performance of a hybrid system based on a solid oxide fuel cell reactor and a micro gas turbine, J. Power Sources 96 (2001) 352–368.
[17] B.H. Bae, J.L. Sohn, S.T. Ro, Thermodynamic modeling and performance analysis of a power generation system based on the solid oxide fuel cell, ASME Paper FUELCELL2003-1735, 2003.
[18] S.C. Singhal, Progress in tubular solid oxide fuel cell technology, Electrochem. Soc. Proc. 99-19 (1997) 39–51.
[19] S.C. Singhal, Advances in solid oxide fuel cell technology, Solid State Ionics 135 (2000) 305–313.
[20] T.W. Song, Performance analysis of the SOFC gas turbine hybrid system with a quasi-2D Model, PhD dissertation, Seoul National University, 2004.
[21] K. Tanaka, C. Wen, K. Yamada, Design and evaluation of combined cycle system with solid oxide fuel cell and gas turbine, Fuel 79 (2000) 1493–1507.
[22] N.F. Bessette, W.J. Wepfer, A mathematical model of a tubular solid oxide fuel cell, J. Energy Resour. Technol. 117 (1995) 43–49.